Statistical Analysis of Relationship between daytime Lidar-Derived Planetary Boundary Layer Height and Relevant Atmospheric Variables in the Semi-Arid Region in Northwest China

Ruijun Dang[1], Hong Li[1], Zhiguo Liu[2], and Yi Yang[1*]

[1] *Key Laboratory of Arid Climatic Changing and Reducing Disaster of Gansu Province, College of Atmospheric Sciences, Lanzhou University, Lanzhou, Gansu 730000, China*

[2] *The Central Meteorological Observatory of Lanzhou , Lanzhou, 730020, China*

Nov 9th, 2015

Submitted to *Advances in Meteorology*

Corresponding author's address:
*Yi Yang (Email: yangyi@lzu.edu.cn, Cell phone: +86-13893256933)
College of Atmospheric Sciences, Lanzhou University, No.222 TianShui South Road, Lanzhou City, Gansu Province 730000, China

Abstract

For boundary layer parameterization and boundary layer height (BLH) assimilation in numerical model, analyzing which atmospheric variables well correlate with BLH and how far the influence radius of variables is in spatial and temporal domain is very meaningful, which can be used to adjust the initial conditions. The daytime BLH on 42 cloudless sunny days from June 2007 to May 2008 over Lanzhou suburb in the Yuzhong area (China) was measured at the Semi-Arid Climate and Environment Observatory of Lanzhou University. BLH was retrieved from Micro Pulse Lidar (MPL-4) data using the curve fitting method, and correlations were calculated between averages, as well as time series of BLH and the atmospheric variables. Most thermal variables (e.g., radiation variables and surface temperature, but not net surface radiation and sensible heat flux) were significantly correlated with BLH about 2–3 hours later. The two highest correlations occurred between surface upward long wave radiation and BLH 3 hours later (r = 0.723, where r is the Pearson correlation coefficient), and between surface temperature (r = 0.704) and BLH 2 hours later, while sensible heat flux significantly correlated with BLH less than 1 hour later (r = 0.629). Surface relative humidity and atmospheric pressure were weaker negatively correlated with BLH. In spatial domain, the correlation between air temperature and BLH was highest (without a lag) near the ground, and decreased with height.

1. Introduction

The atmospheric boundary layer, also known as the planetary boundary layer (PBL), is that part of atmosphere closest to the Earth's surface and is directly affected by the underlying surface conditions and is intimately associated with human activity [1]. The atmosphere is always in a turbulent status, and the transfer of momentum, heat, and moisture between the surface and atmosphere depends on turbulence; consequently, the boundary layer is crucial to surface–atmosphere exchanges of substances and energy. The boundary layer height (BLH) is of major relevance in boundary layer research as a key parameter characterizing the structure of the boundary layer [2, 3]. The height and structure of boundary layer is closely related to the distribution of air temperature and atmospheric stability. Under clear conditions when atmosphere is in neutral or unstable, BLH is more or less identical with the mixed layer height (MLH), which is

defined as the height up to the bottom of the inversion layer that prevents the thermally driven vertical turbulent mixing process. So the gradients of conservative variables such as potential temperature, specific humidity and the concentration of aerosol particle are often regarded as suitable signs to identify the height of mixed layer (also BLH).

Of all indirect methods, lidar is an effective technique for detecting the troposphere, many studies have shown that lidar can be used to provide reasonably accurate estimates of the BLH [4-6]. In recent years, with the intensification of and increasing emphasis on urban pollution, lidar has become much more widely used to detect the urban boundary layer as its detection capabilities have improved [7-9] and because of its high temporal and spatial resolution. In addition, compared with traditional atmospheric detectors, lidar has the advantages of operating over a greater height than sodar and meteorological towers, and providing long-term continuous observation, unlike radiosonde and aircraft platforms. However, the clouds locating at the top of the boundary layer can result in lidar backscatter signal attenuation due to cloud particles, and it is difficult to determine if attenuation is caused by cloud or aerosol gradient [10]. Therefore, in this paper clear sky conditions were chosen to calculate BLH from lidar data.

Retrieving BLH from lidar data uses the gradient of the aerosol particle concentration existing at MLH, as the backscatter signal generally decreases most rapidly at the top of the boundary layer. Many methods have been used to obtain the BLH from backscatter intensity, including the gradient method [11-13], the wavelet transform method [14-16], the standard deviation method [17], and the curve fitting method [18, 19]. Each method has advantages and disadvantages. For example, the gradient method only provides comparatively accurate BLH when the boundary layer varies obviously, if this is not the case or if there is low cloud, obtaining fairly accurate BLH is very difficult [20], while the standard deviation method is not suitable for the situation of weak inversion layer [21]. Although the curve fitting method is relatively computationally expensive, it is insensitive to input parameters and is barely affected by the local structure of the signal, and generally the extracted results are stable. Therefore, for batch processing of large amounts of data, curve fitting is the best method [19] and was used to retrieve daytime BLH in this paper.

In theory, the boundary layer is categorized into the atmospheric thermal boundary layer and the neutral boundary layer, however, the earth's atmosphere mainly behaves as a thermal boundary

layer, and occurrences of a neutral boundary layer are rare. The atmospheric thermal boundary layer is largely governed by land surface processes, including the absorption of solar radiation by the land surface, transmission of heat energy to the atmosphere and soil, and mechanical processes. The surface temperature is an important external forcing for the atmosphere causing convection [22], which depends on the surface heating determined by the radiation budget. The dependence of the net radiation on the long- and shortwave components varies with atmospheric conditions: on sunny days, the upward long wave contributes most to the net radiation, followed by downward shortwave, downward long wave and finally upward shortwave [23]. Besides, the development and maintaining of the thermal boundary layer mainly rely on the heat transmission through the sensible heat flux [24]. Therefore, all the radiation variables, together with surface temperature and sensible heat flux, make major contributions to the formation and development of the boundary layer, and are closely correlated with the BLH [25-28], so it will be meaningful to assimilate the observations of variables that contributes to BLH into the numerical model, and adjust the initial conditions for assimilating BLH, which will provide stronger evidence for boundary layer parameterization and BLH assimilation.

For BLH assimilation in the numerical model, what should be mastered is that which variables well correlate with BLH, as well as how far the influence radius of variables is in the horizontal, vertical directions and in time domain. So the focus of study is to find out the statistical correlation between BLH and conventional atmospheric variables using the routine observations at the Semi-Arid Climate and Environment Observatory of Lanzhou University (SACOL), then provide basis and support for BLH assimilation in northwest China. By the limits of the single observational point, we couldn't find out the radius of influence in horizontal direction. For the vertical direction, we did the work using the vertical air temperature profile provided by a Radiometrics profiling radiometer (TP/WVP-3000). The observations of variables and BLH later some hours were used to analyze the influence radius in time.

Considering the above, the works are as follows: 42 cloudless sunny days (non-precipitation, without thunderstorm, no cloud or total-cloud covers is less than 20 percent all day and with a clear structure of backscatter signals of lidar) were selected from June 2007 to May 2008, and the BLH was calculated by retrieving lidar data using the curve fitting method over the Lanzhou suburb in

the Yuzhong area at SACOL. The correlations between averages of variables and BLH, as well as lagged correlations between time series of variables and BLH were calculated, to determine the major variables affecting the formation and development of boundary layer, the correlation coefficients of BLH and air temperature at different heights were also calculated. Finally, taking 15 July 2007, 20 November 2007, 5 January 2008 and 9 April 2008 as typical examples in different seasons, we investigated the temporal variations in BLH and variables, and discussed specifically how the atmospheric variables affect the development of the boundary layer and the time it takes for the boundary layer to react to changes in the driving variables in different seasons.

2. Data and methods

The BLH and statistical correlations in this paper were calculated from data collected at SACOL (35.946°N, 104.137°E; 1961 m above sea level), which is near the city of Lanzhou on the southern bank of the Yellow River, in a typical semi-arid region. The main instruments providing the data include air temperature and relative humidity (HMP45CL, Vaisalla), a Precision Infrared temperature radiometer (IRTS-P, Apogee), upward and downward pyranometers (CM21, Kipp & Zonen), upward and downward pyrgeometers (CG4, Kipp & Zonen), an atmospheric Pressure Sensor (RPT410F-3143, Druck), a Radiometrics Profiling Radiometer (TP/WVP-3000, Radiometrics), and a Micro-Pulse Lidar system (MPL-4, Sigma Space). The vertical spatial resolution of the radiometer providing air temperature profiles is 100 m below 1 km and 250 m above 1 km. The lidar wavelength is 527 nm, its spatial resolution is 75 m, and the temporal resolution is 30 min. Level 1.0 data are used, which record backscatter intensity from the ground to a height of 10 km. For all the conventional atmospheric variables, after basic quality control process, observations with a relatively high accuracy were selected. The micro-pulse lidar (MPL-4) in SACOL has been a number of the Micro-Pulse Lidar Network (MPLnet) [29] lidars, observations follow the uniform rules of MPL-net. Meanwhile, for lidar data, a series of corrections have been done such as background correction, overlap correction and range correction [30].

The curve fitting method first proposed by Steyn [20] is used to retrieve BLH from the lidar data. The technique uses the gradient of the lidar backscatter signal and fits an idealized backscatter

profile $B(z)$ to the observed backscatter profile $b(z)$ by minimizing the measure of agreement between the two profiles. The form of the idealized backscatter profile $B(z)$ is

$$B(z) = \frac{(B_m + B_u)}{2} - \frac{(B_m - B_u)}{2}\,\mathrm{erf}\left(\frac{z - Z_m}{S}\right),$$

Where B_m and B_u are the mean backscatter in the mixed layer and in air immediately above the mixed layer, respectively; Z_m is the depth of the mixed layer; S is related to the thickness of the entrainment layer [31], which is usually defined to be the layer in which the mixing ratio of boundary layer and overlying air lies in the range 0.05–0.95. The ordinates of the error function thus dictate that entrainment zone thickness $EZT = 2.77 \times S$ [18]. The four parameters are determined by minimizing the root-mean-square difference between the two profiles.

For the technique, what should be considered is that the change of B_m (the mean backscatter in the mixed layer) greatly influences the effect of fitting [19], which may leads to the estimated error of the BLH. Furthermore, although the curve fitting method has advantages to retrieve BLH as described in last section, the technique can only detect boundary layer structures when the aerosols play as targets or tracers for lidar backscatter [18].

3. Statistical correlations between BLH and variables

3.1. Statistical correlations between averages. The dates chosen for BLH retrieval and correlation analysis are listed in Table 1. There are 42 cloudless sunny days with good atmospheric visibility, on which complete observations were made and the backscatter signals have a clear structure. To ensure representativeness, the selected days are from all four seasons, but because there are many cloudy and wet days in autumn, and some data were unavailable for 8–30 September 2007, there are relatively few days in autumn; however, this does not affect the representativeness of the statistical correlations between the atmospheric variables and BLH.

TABLE 1: Selected days for retrieving BLH and for correlation analysis between BLH and atmospheric variables from June 2007 to May 2008

June.	July	Aug.	Nov.	Dec.	Jan.	Feb.	Mar.	Apr.	May.
1	15	14	20	19	5	20	1	2	4
9	16	16	22	20	9	21	3	4	5

22	19	28	22	15		13	6	11
	31	30				25	9	14
						26	17	26
							24	28
							25	31
							27	
							28	

Table 2 lists the Pearson correlation coefficients of the averages of different variables and BLH during 10:00 and 18:00 (Local standard time). It shows strong correlations between individual thermal variables (e.g., surface air temperature, surface temperature, sensible heat flux and upward and downward long wave and shortwave radiation) and BLH, with correlation coefficients all around 0.6 (significant at the 0.01 level). Surface relative humidity and atmospheric pressure are negatively correlated with BLH but their relevance is relatively low (r = –0.339 and –0.247, respectively). The weakest correlation is between net radiation and BLH. The distribution of averages of variables and BLH are plotted in Figure 1, showing little change in the daily average of net radiation (Figure 1(b)), whereas the BLH shows a clear change. The overall trends of atmospheric pressure and surface relative humidity are generally opposite to that of BLH although they change in tandem with BLH some times. Apart from these three variables, the overall trends are fairly consistent with the trend of BLH.

TABLE 2: Statistical correlations between the averages of atmospheric variables and boundary layer height from 10:00 to 18:00 (SAT: surface air temperature; ST: surface temperature; SHF: sensible heat flux; SRH: surface relative humidity; AP: atmospheric pressure; ULR, USR, DLR, DSR: upward long wave and shortwave radiation, and downward long wave and shortwave radiation, respectively; NR: net radiation; r: Pearson correlation coefficient; l: level of significance)

variables	*R*	*L*
SAT	0.707**	0.000
ST	0.711**	0.000
SHF	0.629**	0.000
SRH	-0.339*	0.028
AP	-0.247	0.114
ULR	0.753**	0.000
DLR	0.545**	0.000

DSR	0.764**	0.000
USR	0.599**	0.000
NR	-0.043	0.788

*Significant correlation at the 0.05 level

**Significant correlation at the 0.01 level

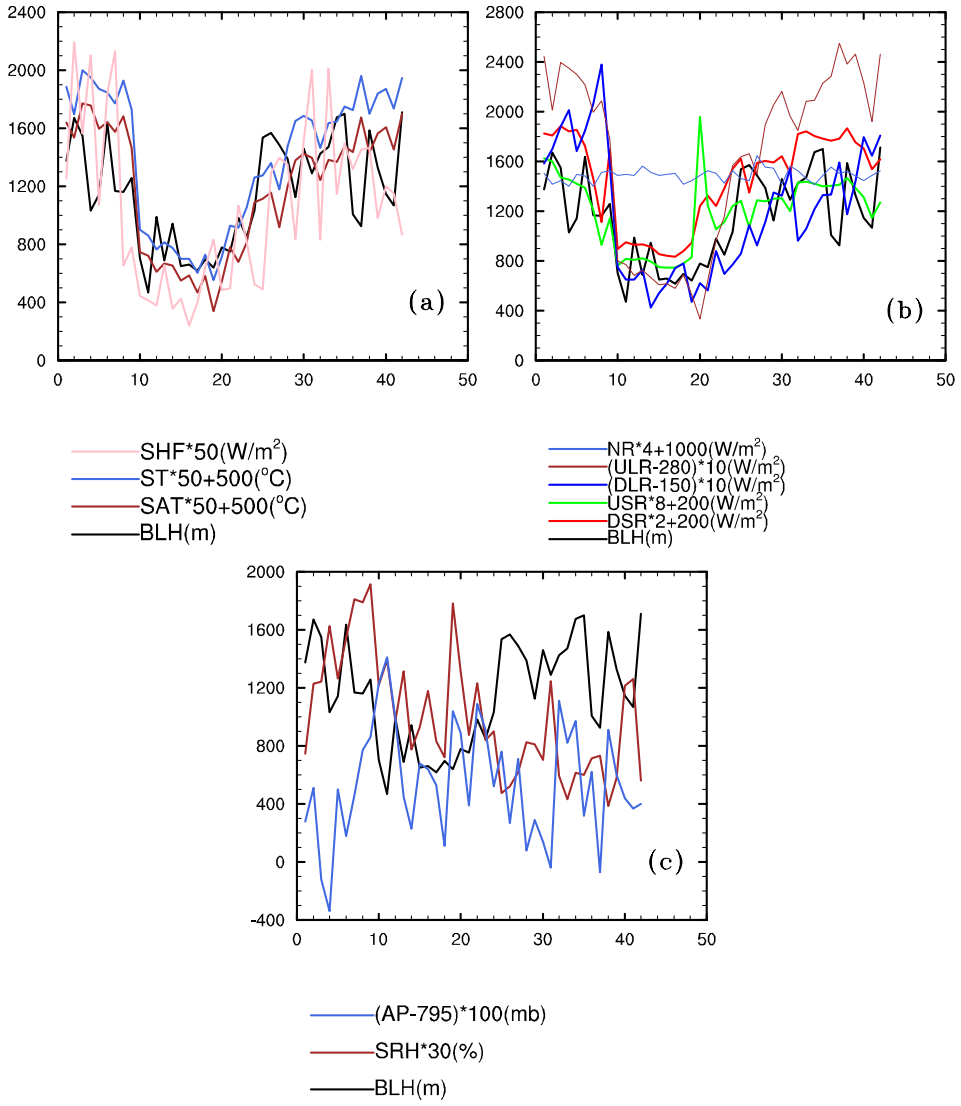

FIGURE 1: Distribution of averages of atmospheric variables and boundary layer height (see Table 2 for abbreviations).

3.2. Statistical correlations between time series. In general, the atmospheric boundary layer appears as a daytime convective layer and a stable boundary layer at night. As discussed by Ding [32] that the boundary layer is relatively stable before sunrise in northwest China, with a thick mixed layer. After 08:00, the nighttime stable boundary layer breaks up, and the mixed layer starts to deepen; around 10:00, it begins to develop rapidly and the residual layer starts to disappear because of

thermally driven vertical mixing; the convective boundary layer is established by noon. Zhao [33] estimated the BLH in summer over the SACOL using lidar measurements and a numerical model, and showed that the deepest boundary layer over SACOL occurs at around 17:00 and can last until 18:00. Therefore, BLH was selected every 30 minutes during 10:00–18:00, and atmospheric variables were selected during 06:00–14:00, 07:00–15:00, 08:00–16:00, 09:00–17:00, and 10:00–18:00 as time series to analyze the lagged statistical correlations between variables and BLH, as the boundary layer often develops after changes in these variables.

Statistical correlations between different atmospheric variables and BLH with a lag of 1, 2, 3, and 4 hours are listed in Table 3. There are significant correlations between thermal variables (except net radiation) and BLH, with Pearson correlation coefficients all above 0.6 (significant at the 0.01 level), which is highly consistent with the results shown in Table 2. It is also clear that stronger significant correlations exist between variables and the BLH 2–3 hours later. The Pearson correlation coefficients between surface temperature, surface air temperature and BLH 2 hours later are 0.704 and 0.677. Upward long wave radiation, upward shortwave radiation, and downward shortwave radiation are more highly correlated with BLH 3 hours later, with correlation coefficients of 0.723, 0.687, 0.608, respectively; downward long wave radiation is different from the others and is more highly correlated with BLH measured at the same time. Besides, with the correlation coefficient of 0.629, sensible heat flux highly correlates with BLH at the same time or later about 1 hour. The weakest correlation of the radiation variables is between net radiation and BLH; here, the strongest correlation is with BLH 3 hours later. Atmospheric pressure and surface relative humidity are both negatively correlated with BLH although the correlation is not as significant as the case of the thermal variables; the BLH changes about 2 hours after a change in relative humidity.

TABLE 3: Statistical correlations between different atmospheric variables and boundary layer height at lag time of 1–4 hours (SAT: surface air temperature; ST: surface temperature; SHF: sensible heat flux; SRH: surface relative humidity; AP: atmospheric pressure; ULR, USR, DLR, DSR: upward long wave and shortwave radiation, and downward long wave and shortwave radiation, respectively; NR: net radiation; *r*: Pearson correlation coefficients; *l*: Significance level)

variables	At same time		BLH later 1 h		BLH later 2 h		BLH later 3 h		BLH later 4 h	
	r	*l*	*r*	*L*	*r*	*l*	*r*	*l*	*r*	*L*
SAT	0.647**	0.000	0.667**	0.000	0.677**	0.000	0.677**	0.000	0.666**	0.000
ST	0.677**	0.000	0.697**	0.000	0.704**	0.000	0.701**	0.000	0.684**	0.000
SHF	0.629**	0.000	0.627**	0.000	0.605**	0.000	0.570**	0.000	0.518**	0.000
SRH	-0.414**	0.000	-0.428**	0.000	-0.427**	0.000	-0.412**	0.000	-0.374**	0.000
AP	-0.311**	0.000	-0.290**	0.000	-0.251**	0.000	-0.202**	0.000	-0.156**	0.000
ULR	0.569**	0.000	0.669**	0.000	0.716**	0.000	0.723**	0.000	0.709**	0.000
DLR	0.507**	0.000	0.506**	0.000	0.499**	0.000	0.480**	0.000	0.461**	0.000
DSR	0.285**	0.000	0.544**	0.000	0.676**	0.000	0.687**	0.000	0.657**	0.000
USR	0.170**	0.000	0.406**	0.000	0.565**	0.000	0.608**	0.000	0.602**	0.000
NR	-0.147**	0.000	0.179**	0.000	0.403**	0.000	0.452**	0.000	0.428**	0.000

*Significant correlation at the 0.05 level

**Significant correlation at the 0.01 level

To identify any relations and influence radius in the vertical direction, the statistical correlations between BLH and air temperature at different heights and at different times are listed in Table 4. At 10:00, only air temperature below 1000 m is correlated with BLH, but after 12:00, air temperature within 5000 m is significantly correlated with BLH. Thermal forcing is the driving force for the development of mixing layer in daytime (10:00-18:00), but only small amount of solar radiation is absorbed by air in the boundary layer, most (about 90%) are delivered to the surface, then the surface varies responding to the solar radiation changes and forces the changes of boundary layer through turbulent transport, the forcing effect decreases with height, and the higher altitude, the less significant temporal variation of air temperature [1], that' why the Pearson correlation coefficient is highest at the surface and decreases with height at all times. Furthermore, the highest correlation between BLH and air temperature below (above) 1000 m occurs at 12:00 (14:00) with a Pearson correlation coefficient of 0.748 (0.637), for the whole troposphere, the ground surface is the main heat source, the air temperature in the free atmosphere also changes with the surface variation, that is, variation of solar radiation, so there is no doubt that relative higher correlation exits between BLH and air temperature at even 5 km at 14:00.

TABLE 4: Statistical correlations between BLH and air temperature at different heights and at different times (*r*: Pearson correlation coefficient; *l*: Significance level)

height	10:00	12:00	14:00	16:00	18:00

(m)	*r*	*l*	*r*	*L*	*r*	*L*	*r*	*l*	*r*	*L*
0	0.565**	0.000	0.748**	0.000	0.655**	0.000	0.638**	0.000	0.627**	0.000
100	0.545**	0.000	0.739**	0.000	0.655**	0.000	0.639**	0.000	0.617**	0.000
200	0.532**	0.000	0.727**	0.000	0.654**	0.000	0.632**	0.000	0.608**	0.000
300	0.519**	0.000	0.718**	0.000	0.653**	0.000	0.623**	0.000	0.601**	0.000
400	0.481**	0.000	0.708**	0.000	0.652**	0.000	0.610**	0.000	0.590**	0.000
500	0.446**	0.003	0.697**	0.000	0.647**	0.000	0.599**	0.000	0.582**	0.000
600	0.412**	0.007	0.683**	0.000	0.644**	0.000	0.585**	0.000	0.571**	0.000
700	0.385*	0.012	0.668**	0.000	0.642**	0.000	0.573**	0.000	0.558**	0.000
800	0.360*	0.019	0.654**	0.000	0.640**	0.000	0.563**	0.000	0.548**	0.000
900	0.341*	0.027	0.641**	0.000	0.639**	0.000	0.553**	0.000	0.539**	0.000
1000	0.322*	0.038	0.629**	0.000	0.637**	0.000	0.540**	0.000	0.529**	0.000
1250	0.275	0.078	0.592**	0.000	0.628**	0.000	0.5000**	0.001	0.496**	0.001
1500	0.252	0.108	0.575**	0.000	0.625**	0.000	0.477**	0.001	0.478**	0.001
1750	0.256	0.101	0.573**	0.000	0.627**	0.000	0.478**	0.001	0.475**	0.001
2000	0.255	0.103	0.565**	0.000	0.625**	0.000	0.470**	0.002	0.469**	0.002
2250	0.254	0.105	0.558**	0.000	0.624**	0.000	0.462**	0.002	0.460**	0.002
2500	0.257	0.101	0.557**	0.000	0.623**	0.000	0.458**	0.002	0.456**	0.002
2750	0.249	0.112	0.547**	0.000	0.618**	0.000	0.447**	0.003	0.446**	0.003
3000	0.256	0.102	0.551**	0.000	0.620**	0.000	0.447**	0.003	0.448**	0.003
3250	0.245	0.118	0.539**	0.000	0.611**	0.000	0.431**	0.004	0.432**	0.004
3500	0.247	0.115	0.537**	0.000	0.609**	0.000	0.427**	0.005	0.427**	0.005
3750	0.242	0.123	0.531**	0.000	0.604**	0.000	0.417**	0.006	0.419**	0.006
4000	0.251	0.109	0.534**	0.000	0.604**	0.000	0.420**	0.006	0.422**	0.005
4250	0.252	0.107	0.533**	0.000	0.600**	0.000	0.416**	0.006	0.419**	0.006
4500	0.250	0.111	0.530**	0.000	0.598**	0.000	0.412**	0.007	0.414**	0.006
4750	0.246	0.117	0.527**	0.000	0.595**	0.000	0.407**	0.007	0.409**	0.007
5000	0.247	0.115	0.528**	0.000	0.594**	0.000	0.408**	0.007	0.409**	0.007

*Significant correlation at the 0.05 level

**Significant correlation at the 0.01 level

4. Cases analysis

To verify the statistical results and analyze the roles played by atmospheric variables in the development of the boundary layer, four cloudless sunny days from different seasons, 15 July 2007, 20 November 2007, 5 January 2008 and 09 April 2008, were selected as typical summer, fall, winter and spring examples for analysis.

4.1 Synoptic condition. Besides surface processes, synoptic condition is also an important factor contributing to the overall height of boundary layer. The surface pressure at 14:00 Beijing time on 9 April 2008, 15 July 2007, 20 November 2007 and 5 January 2008 are shown in figure 2, while Figure 3 shows the time–altitude cross-section of the backscatter intensity and temporal variation in BLH retrieved using the curve fitting method (red line). After 10:00, BLH began to increase on all

cases, higher BLH appeared before 10:00 on 9 April 2008 and 15 July 2007 (Figure3 (a), (b)), which may be caused by cloud or the inherent disadvantage of the method. Figure 2 (a) and (b) shows that at 14:00, on 9 April 2008 and 15 July 2007, Yuzhong region was controlled by weak low-surface pressure, the updrafts promoted boundary development, and according to Figure 3 (a) and (b), the highest BLH were 1850 m and 2150 m on the two cloudless sunny days, which were relative higher than on other two cases. On 20 November 2007 and 5 January 2008, the area was controlled by the edge of high-pressure system at 14:00 Beijing time, indicating aloft airflow convergence and surface divergence, which subsided and restricted the development of BLH, and the highest BLH were 1100m and 860 m on the two cases (Figure 3 (c) and (d)). Meanwhile, Figure 3 shows that difference exited on the time that BLH got the maximum, on 09 April 2008 and 15 July 2007, the BLH increased to the peak at 17:30 and 15:30, while on 20 November 2007 and 5 January 2008, the BLH got the maximum at 17:00. It is not difficult to understand that the difference on temporal variation in BLH is closely related to the differences on the land surface processes and the variation in atmospheric variables. In addition, the difference between the height at which the signal reduced fastest and the BLH (retrieved with the curve fitting method) was small (Figure 3), the corresponding time was also fairly consistent, which supports the choice of the curve fitting method for retrieving BLH on sunny days.

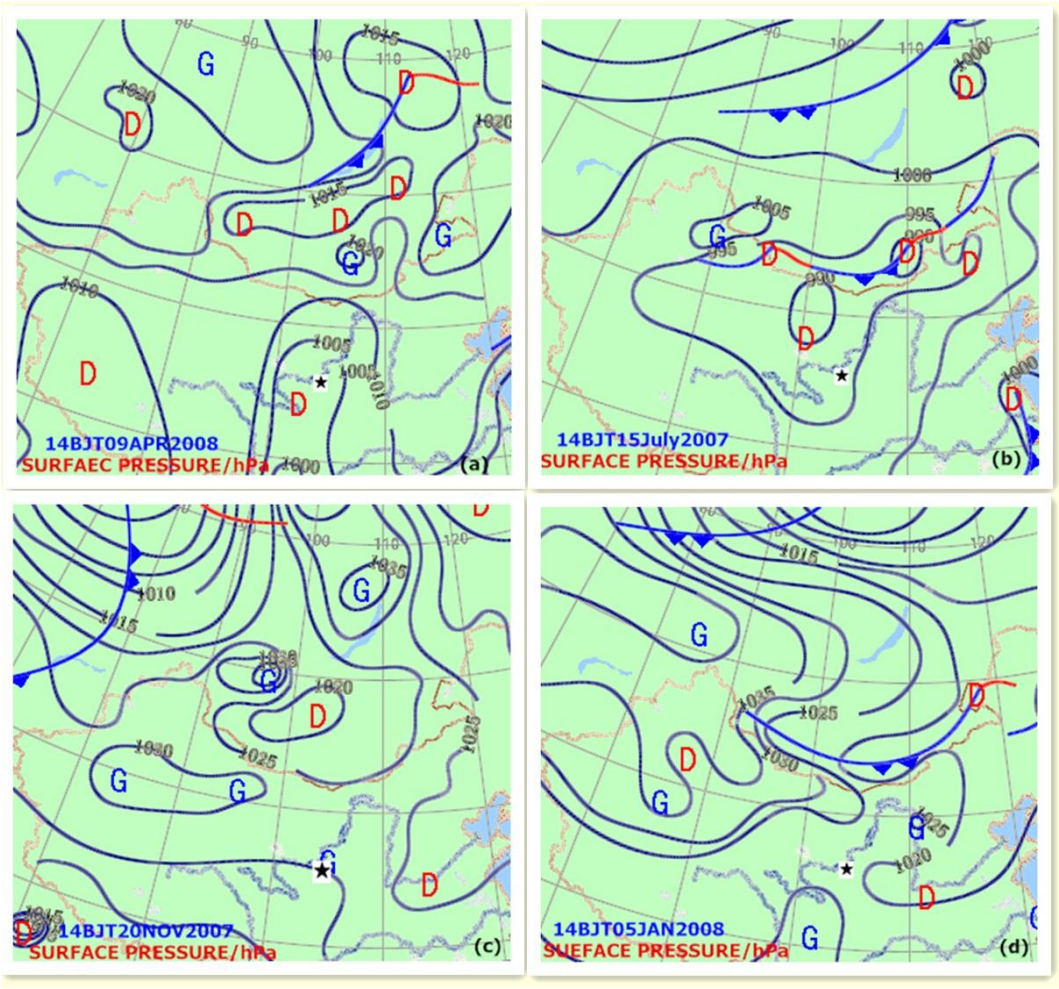

282

283 FIGURE 2: Surface pressure at (a) 14:00 BJT 9 April 2008, (b) 14:00 BJT 15 July 2007, (c) 14:00

284 BJT 20 November 2007, and (d) 14:00 BJT 5 January 2008. Black star denotes measurement site.

285

286

287

288

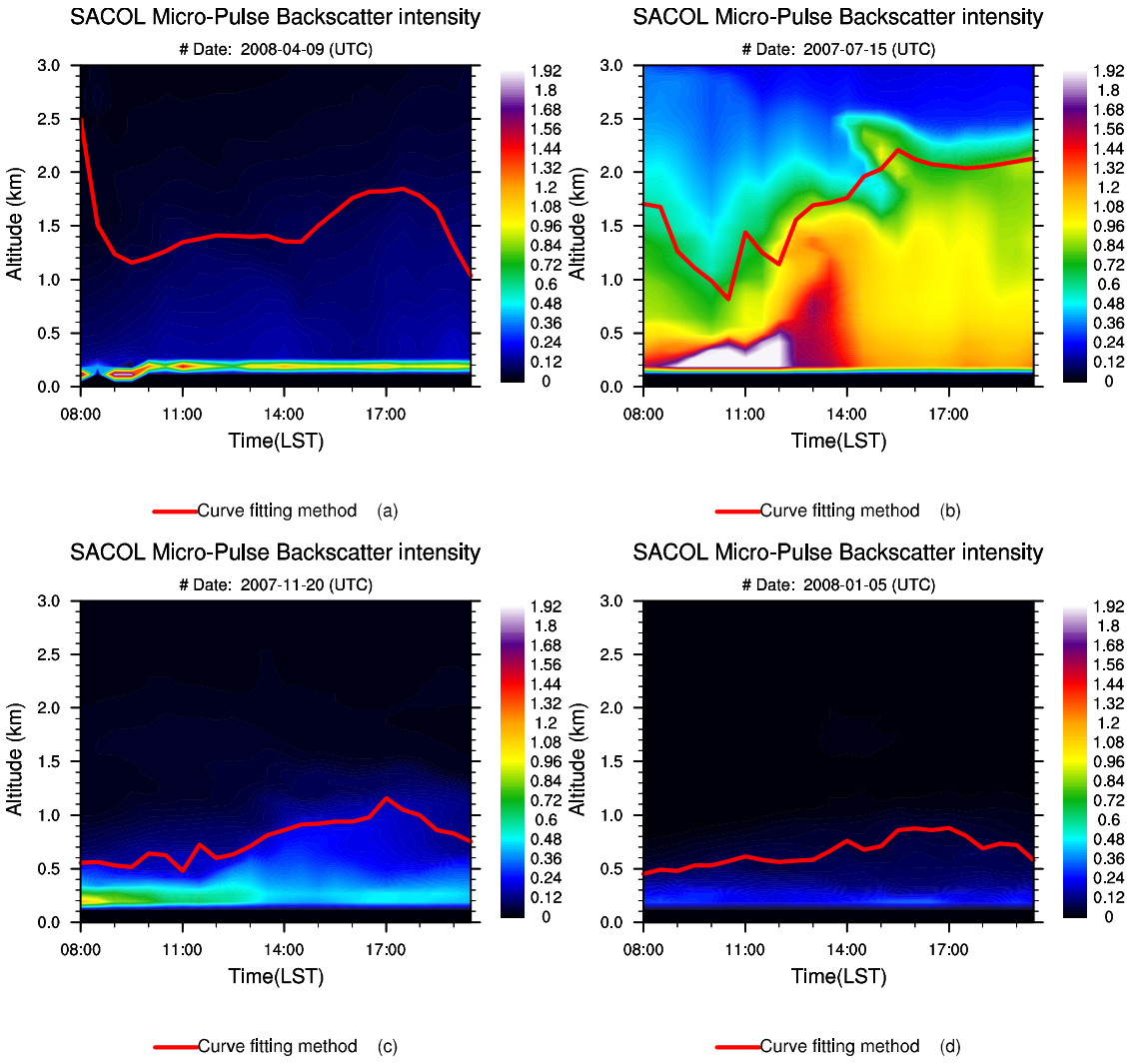

FIGURE 3: Time–altitude cross-sections of the backscatter on (a) 9 April 2008, (b) 15 July 2007, (c) 20 November 2007, and (d) 5 January 2008.

4.2 Temporal variation analysis. The temporal variations in radiation variables are plotted in Figure 4. The downward shortwave radiation (DSR) is the part of the solar radiation that reaches the surface after attenuation by the atmosphere, some is absorbed by the surface and the rest is reflected back into the atmosphere as upward shortwave radiation (USR). Therefore, on all cases, although had a lower intensity, the upward shortwave radiation always accompanied the downward component. From Figure 4, it is obviously that on the first two cases, short wave radiation had higher values than on the 20 November 2007 and 5 January 2008, which were caused by the seasonal variation of solar altitude angles (atmospheric transparency was not considered in cloudless sunny days). Except the synoptic condition, shortwave radiation contributes to the difference on BLH to a certain extent as the ultimate source of energy. Besides, for temporal

variation, the two variations reached their maximum values between 12:30 and 13:30, at about 13:00 on 15 July 2007 and 12:30 on 20 November 2007, while at about13:30 on 9 April 2008 and 5 January 2008, and then decreased rapidly. Although the temporal variation in shortwave radiation was similar, significant difference exited on the development and lag time of BLH on four cases: the lag time of BLH was less than 3 hours on 15 July 2007, while BLH developed more than 3 hours later on other three cases, indicating that differences on land process in different seasons contributes to the difference on the lag law of BLH.

The upward long wave radiation (ULR) changed 0.5 to 1 hour later than the shortwave radiation, this is because upward long wave radiation depends on surface temperature, and the various processes occurring from the arrival of solar radiation at the surface to the surface reaching its maximum temperature take some time. Obviously the biggest value of the upward long wave radiation was on 15 July 2007 while the smallest one on 5 January 2008, on other two cases was somewhere in between. The times that the peaks occurred were between 13:30 to 14:30, indicating that the lag times of BLH were 3.5, 1.5, 3.5 and 2.5 hours respectively. The temporal variation in downward long wave radiation (DLR) was different from that of the other radiation components: increased until about 18:00 or after 17:00 the decreasing tendency began to appear, the temporal variation range of downward long wave radiation was weak on all cases. The atmosphere absorbs both shortwave and long wave radiation, but mainly long wave radiation: only 15%–25% of the shortwave radiation is absorbed. After the long wave radiation is absorbed by greenhouse gases such as water vapor and carbon dioxide, the atmosphere is exothermic, and this is the source of downward long wave radiation; therefore, it is easy to understand why it reached the peak latest. It is also strongly influenced by cloudiness and air humidity, so the intensity of downward long wave radiation was relatively low and it had a weak effect on surface heating on cloudless sunny days, which explains why downward long wave radiation was weaker related to BLH than the other three radiation variables (Table 2).

Figure 4 also shows net radiation (NR), being different from the profile of daily average in Figure 1, it had an obvious daily variation and changed consistently with shortwave radiation on all cases. The variation in net radiation is the cumulative results of the components' variation in the radiation balance, but the shortwave radiation is the dominant variable. The major factors that

affect the net radiation are solar altitude angles, altitude, cloud cover and surface albedo (altitude and cloud cover, not considered in the study), so the variation of solar altitude angles on the different cases is the fundamental factor to the difference of net radiation [34], and the lagged law between net radiation and BLH on different cases is similar to that between the shortwave radiation and BLH.

Figure 5 shows temporal variations in surface air temperature (SAT), surface infrared temperature (ST), sensible heat flux (SHF) and surface wind speed (WS). The surface air temperature was the air temperature at 2 meters above the surface, so it changed basically synchronously with the surface temperature. Relative to two temperature variables, except 15 July 2007, BLH showed significant lag on other three cases, the lag time was about 1 hour on 17 April 2008, about 2 hours on 20 November 2007 and 1 January 2008. On 15 July 2007, two profiles of temperature increased until about 17:00 and then began to decrease, which were in line with the trend of BLH and didn't show the lag effect of BLH very well, which may be responding to that in summer turbulent exchange is stronger and heat exchange between surface and atmosphere is faster. The temporal variation in sensible heat flux (SHF) was different from others, especially on the previous two cases it even changed simultaneously with BLH, on 20 November 2007 and 5 January 2008, BLH changed about 1 hour later than the variable. The sensible heat flux is mainly determined by difference between surface temperature, surface air temperature, and surface wind speed. According to Figure 5, the heat sensible flux changed a little time later than the difference between surface temperature and surface air temperature, but wind speed (red lines) kept increasing until 18:00, which led to the less lag time between BLH and sensible heat flux. Besides that, the heat sensible was calculated through surface air temperature, surface temperature and surface wind speed, the accumulated error was inevitable.

The temporal variations in atmospheric pressure (AP) and surface relative humidity (SRH) are shown in Figure 6, opposite to the variation in BLH. A comparison with the surface air temperature in Figure 5 shows that the air temperature reached its maximum at the same time as relative humidity reached its minimum, and the two quantities were highly negatively correlated. Similarly, the lag time was about 1, 2, 2 hours on 17 April 2008, 20 November 2007 and 1 January 2008 respectively. On 15 July 2007, both variables decreased until about 16:00 when relative humidity

maintained its minimum and the tendency of the growth appeared at about 17:00, while pressure kept decreasing until 18:00. In theory, the local atmospheric pressure is mainly determined by surface air temperature: the higher the air temperature, the greater the diffusion of air molecules and the lower the pressure, explaining why pressure and humidity are negatively related with BLH. For the temporal variation, the atmospheric pressure changed weakly and the correlation between it and BLH was not as strong as between BLH and surface air temperature.

The above results show that on all cases in different seasons, the temporal variations in all variables corresponded well to that of BLH, with upward long wave radiation, surface temperature, and surface air temperature having the closest correspondence. In time domain, on different cases difference exited on lag time of BLH, but on the whole, the BLH changed about 3 hours later than shortwave radiation and net radiation; for upward long wave radiation, BLH lagged that 2.5-3 hours, similarly, relative to the surface temperature, surface air temperature and surface relative humidity, BLH developed about 2 hours later; Besides, the BLH changed less than1 hour later than sensible heat flux. The atmospheric pressure changed consistently with BLH on all cases. The difference about lagged effect is mainly because of the seasonal variation of solar altitude angles and as turbulent exchange intensity is different in different seasons. Furthermore, these delays in boundary layer response are related not only to the finite response times of the distribution, transformation, and transmission in the atmosphere for surface radiation energy, but also to the lag in aerosol delivery. For the lidar data, BLH is identified by the vertical distribution of aerosol, but upward transport of aerosol only begins after the boundary layer has developed in response to thermodynamic factors after sunrise, and the true height of the boundary layer declines rapidly with the weakening of solar radiation in the afternoon, whereas the BLH retrieved from lidar data decreased slowly. Delays in boundary layer response may also reflect the influence of dynamical factors such as wind shear. Northwest China is in a region dominated by westerlies, and the atmospheric circulation background that influences the formation and development of the boundary layer has some special characteristics [35]. However, the correlation between wind shear and BLH was not considered because of the limitations of the wind data.

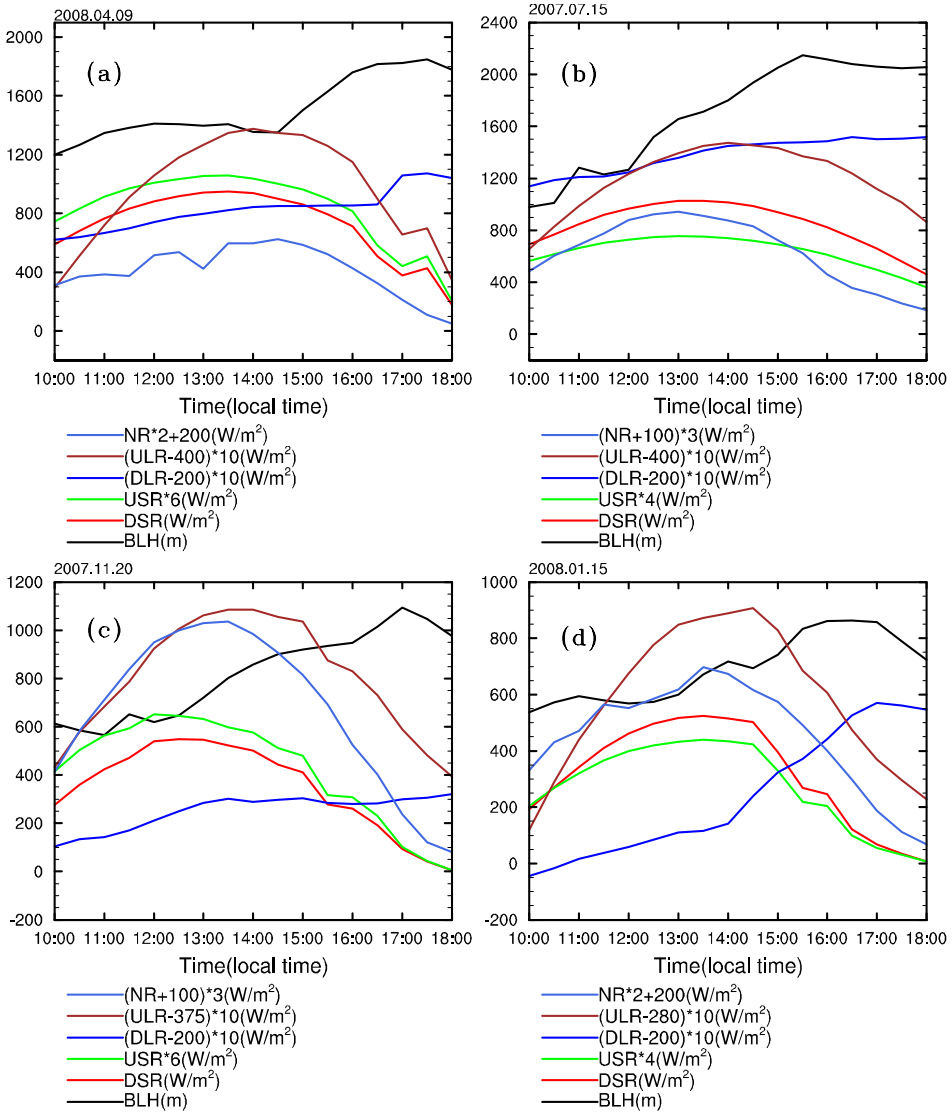

FIGURE 4: Temporal variations in boundary layer height (BLH), downward shortwave radiation (DSR), upward shortwave radiation (USR), downward long wave radiation (DLR), upward long wave radiation (ULR), and net radiation (NR) on (a) 9 April 2008, (b) 15 July 2007, (c) 20 November 2007, and (d) 5 January 2008.

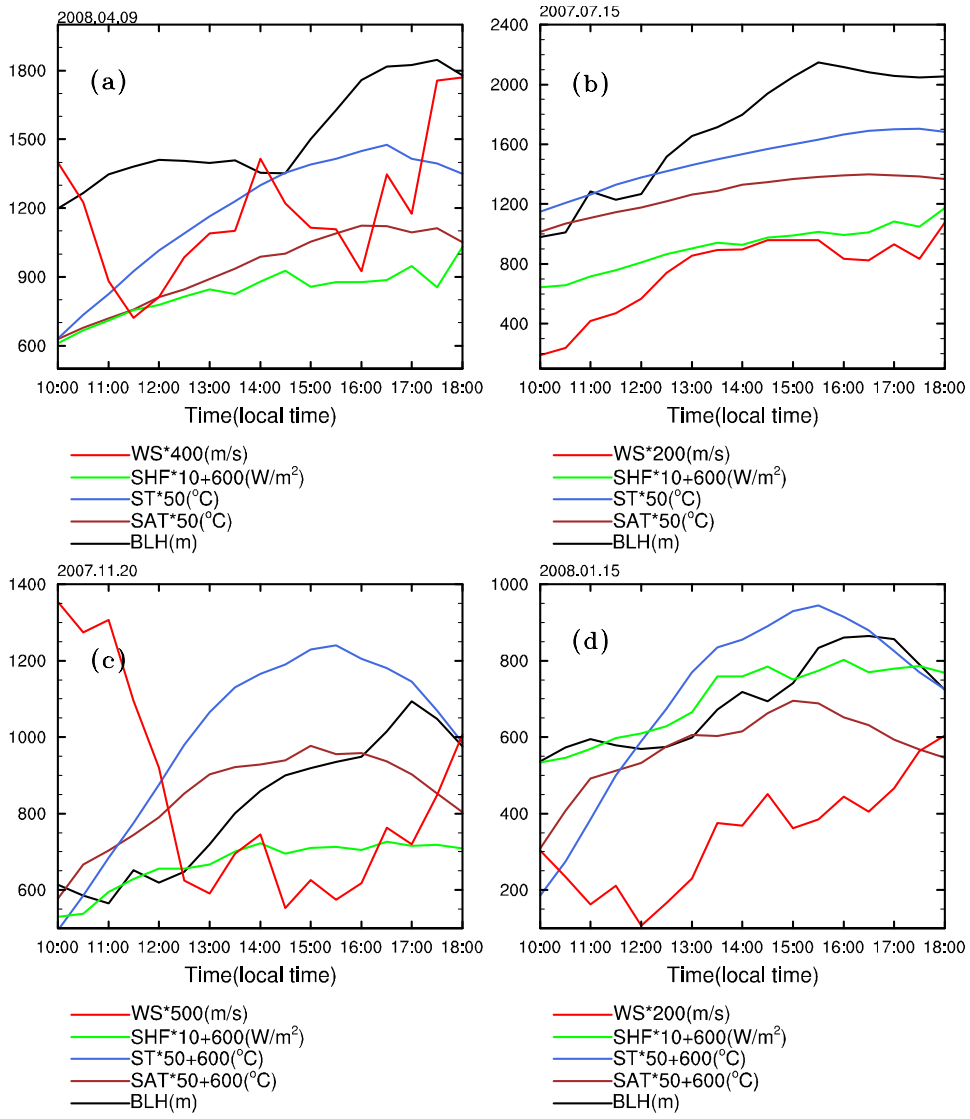

394

395 FIGURE 5: Temporal variations in boundary layer height (BLH), sensible heat flux (SHF), surface

396 temperature (ST), surface air temperature (SAT) and surface wind speed (WS) on (a) 9 April 2008,

397 (b) 15 July 2007, (c) 20 November 2007, and (d) 5 January 2008.

398

399

400

401

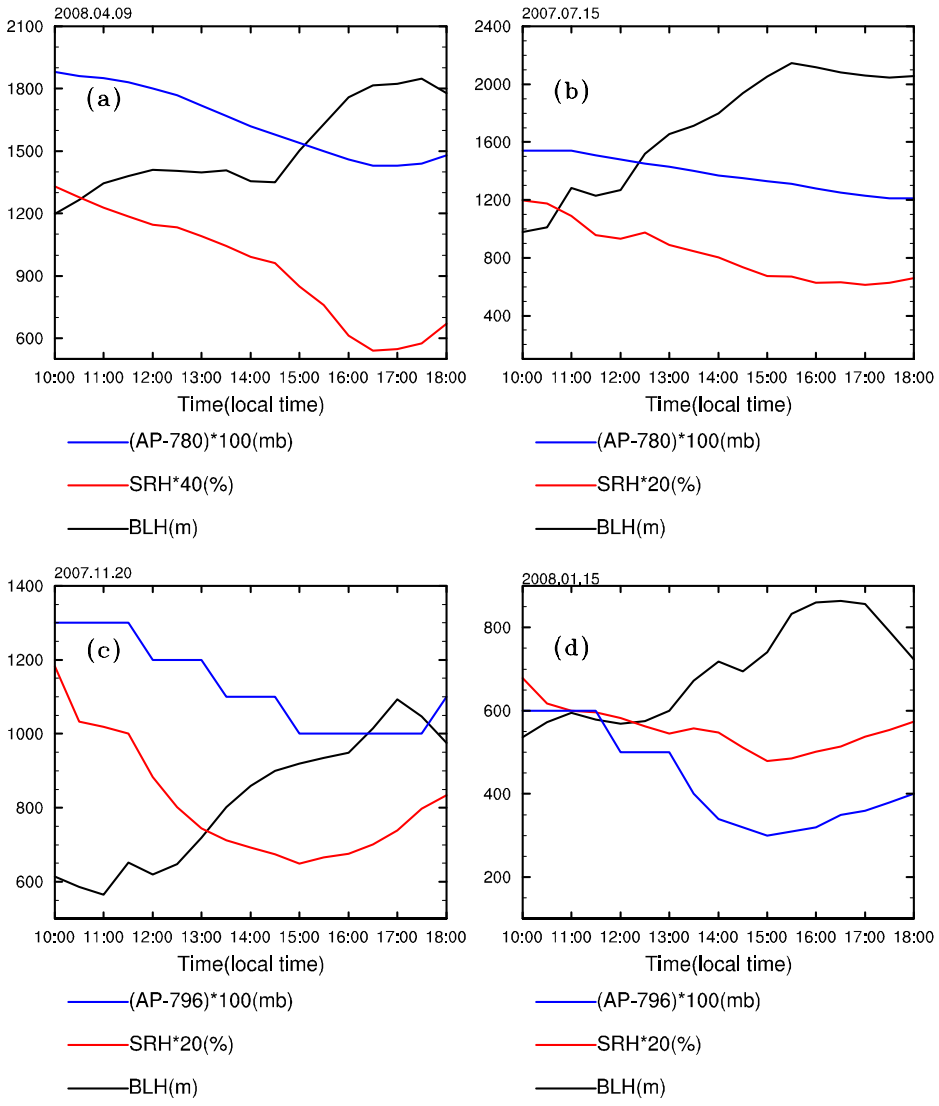

FIGURE 6: Temporal variations in boundary layer height (BLH), surface relative humidity (SRH), and atmospheric pressure (AP) on (a) 9 April 2008, (b) 15 July 2007, (c) 20 November 2007, and (d) 5 January 2008.

5. Conclusions

This study retrieved BLH on cloudless sunny days from June 2007 to May 2008 from lidar data using a curve fitting method, and identified correlations between both averages and time series of BLH and various atmospheric variables; the vertical dependence of BLH on air temperature was also investigated. Then, using four typical cases in different seasons studies 15 July 2007, 20 November 2007, 5 January 2008 and 9 April 2008, the variables responsible for the development of

412 the boundary layer and the lagged correlations between temporal changes of these variables and
413 BLH were investigated. The conclusions of the study are as follows.
414 (1) Among the atmospheric variables (not including dynamic factors), thermal variables such
415 as radiation variables surface temperature and sensible heat flux have more significant positive
416 correlations with BLH. The response time to thermal forcing of the surface and atmosphere,
417 together with aerosol transmission delay, means that the development of the boundary layer lags
418 behind changes in the driving variables, with different lag times for different variables.
419 (2) On different cases, the lag correlation laws between BLH and variables are different
420 (especially on 15 July 2007), but on the whole, only downward long wave radiation changes
421 synchronous with BLH. Changes in the boundary layer occur 3 hours later than changes in
422 downward, upward shortwave radiation, upward long wave radiation and net radiation. The lag
423 time of BLH is about 2 hours relative to surface temperature and surface air temperature, and BLH
424 lags about 1 hour than surface sensible heat flux.
425 (3) Surface relative humidity and atmospheric pressure are weaker negatively correlated with
426 BLH, BLH changes about 2 hours later than surface relative humidity.
427 (4) The vertical dependence of BLH on air temperature is greatest near the surface and
428 decreases with height. The most significant correlation between air temperature below (above)
429 1000 m and BLH occurs at 12:00 (14:00).
430 While these conclusions are important, there are still many unresolved problems. Firstly, curve
431 fitting is an effective method for calculating BLH from lidar data, but is limited to cloudless sunny
432 days. The number of days and their seasonal distribution were constrained by data availability, so
433 while the statistical results are representative they also have some limitations. Secondly, although
434 wind shear, a major dynamical factor, affects the thermal transmission and diffusion capacity of the
435 atmosphere and is significantly correlated with the development of the boundary layer in theory, it
436 was not considered here because of the limited amount of data available. This analysis focused on
437 finding out the statistical correlation between BLH and conventional atmospheric variables
438 according to the directly routine observations at SACOL to provide basis and support for the
439 assimilation of BLH in northwest China, it was not possible enough to comprehensively

characterize the meteorological conditions affecting the development of the boundary layer in the Yuzhong area.

Conflict of Interests

The authors declare that there is no conflict of interests of regarding the publication of this paper.

Acknowledgements

We would like to thank the Semi-Arid Climate and Environment Observatory of Lanzhou University (SACOL) for providing the observation data. This research was supported by the National Natural science Foundation of China (Grant no. 41375109) and Arid Meteorology science Foundation of Institute of Arid Meteorology, China Meteorological Administration (Grant no. IAM201513).

References

[1] R. B. Stull, *An introduction to boundary layer meteorology*, Springer Science & Business Media, 1988.

[2] Q. Zhang, "Review of Atmospheric Boundary Layer Meteorology," *Arid Meteorology*, vol. 21, no. 3, pp. 0074-0078, 2003.

[3] X. M. Hu, J. W. Nielsen-Gammon, and F. Zhang, "Evaluation of three planetary boundary layer schemes in the WRF model," *Journal of Applied Meteorology and Climatology*, vol. 49, no. 9, pp. 1831-1844, 2010.

[4] T. Murayama, H. Okamoto, N. Kaneyasu et al., "Application of lidar depolarization measurement in the atmospheric boundary layer: Effects of dust and sea-salt particles," *Journal of Geophysical Research*, vol. 104, no. 24, pp. 31781-31792, 1999.

[5] C. J. Grund, R. M. Banata, J. L. George et al., "High-resolution Doppler lidar for boundary layer and cloud research," *Journal of Atmospheric and Oceanic Technology*, vol. 18, no. 3, pp. 376-393, 2001.

[6] B. Hennemuth and A. Lammert, "Determination of the atmospheric boundary layer height from radiosonde and lidar backscatter," *Boundary-Layer Meteorology*, vol. 120, no. 1, pp. 181-200, 2006.

[7] M. Mao, W. Jiang, and X. Wu, "Lidar exploring of the UBL in downtown of the Nanjing City," *Acta Science Circumstantiae*, vol. 26, no. 10, pp. 1723-1728, 2006.

[8] H. Wang, T. Cao, J. He et al., "Characteristics Study of Atmospheric Boundary Layer by Mie Scattering Lidar in Chengdu," *Journal of Atmospheric and Environmental Optics*, vol. 2, no. 5, pp. 340-344, 2007.

[9] B. Guo, Q. He, C Li et al., "Remote Sensing Study of a Dust Event over Dalian," *Journal of Nanjing Institute of Meteorology*, vol. 31, no. 5, pp. 624-632, 2008.

[10] E. L. McGrath-Spangler and A. S. Denning, "Estimates of North American summertime planetary boundary layer depths derived from space-borne lidar," *Journal of Geophysical Research Atmospheres*, vol. 117, no. 15, pp. 1984-2012, 2012.

[11] K. L. Hayden, K. G. Anlauf, R. M. Hoff et al., "The vertical chemical and meteorological structure of the boundary layer in the Lower Fraser Valley during Pacific'93," *Atmospheric Environment*, vol. 31, no. 14, pp. 2089-2105, 1997.

[12] V. Wulfmeyer, "Investigation of turbulent processes in the lower troposphere with water vapor DIAL and radar-RASS," *Journal of the atmospheric sciences*, vol. 56, no. 8, pp. 1055-1076, 1999.

[13] J. Huang and J. Wu, "MW-FRA and its pump optimization," *Study of Optical Communication*, no. 2, pp. 53-55, 2005.

[14] S. A. Cohn and W. M. Angevine, "Boundary layer height and entrainment zone thickness measured by lidars and wind-profiling radars," *Journal of Applied Meteorology*, vol. 39, no. 8, pp. 1233-1247, 2000.

[15] I. M. Brooks, "Finding boundary layer top: Application of a wavelet covariance transform to lidar backscatter profiles," *Journal of Atmospheric and Oceanic Technology*, vol. 20, no. 8, pp. 1092-1105, 2003.

[16] H. Li, Y. Ma, and Y. Yang, "Study on Retrieval of Boundary Layer Using Wavelet Transformation Method Based on Lidar Data," *Arid Meteorology*, vol. 33, no. 1, pp. 78-88, 2015.

[17] W. P. Hooper and E. W. Eloranta, "Lidar measurements of wind in the planetary boundary layer: the method, accuracy and results from joint measurements with radiosonde and kytoon," *Journal of climate and applied meteorology*, vol. 25, no. 7, pp. 990-1001, 1986.

[18] D. G. Steyn, M. Baldi, and R. M. Hoff, "The detection of mixed layer depth and entrainment zone thickness from lidar backscatter profiles," *Journal of Atmospheric and Oceanic Technology*, vol. 16, no. 7, pp. 953-959, 1999.

[19] L. Wang, C. Xie, Y. Han et al., "Comparison of Retrieval Methods of Planetary Boundary Layer Height from Lidar Data," *Journal of Atmospheric and Environmental Optics*, vol. 7, no. 4, pp. 241-247, 2012.

[20] L. Wang, C. Xie, Z. Wang et al., "Application of Gradient Method to Detect Height Distribution of Atmospheric Boundary Layer with Lidar," *Journal of Atmospheric and Environmental Optics*, vol. 7, no. 3, pp. 161-167, 2012.

[21] C. Huang, x. Song, and Z. Liu, "Development of Atmospheric Boundary Layer Detection based on Lidar Data", 2012.

[22] Y. Hu and Y. Gao, "Some New Understandings of Processes at the Land Surface in Arid Area from the HEIFE," *Acta meteorologica Sinica*, vol. 525, no. 3, pp. 285-296, 1994.

500 [23] T. Tang, L. Wang, and X. Wen, "A Study of the Radiation and Surface Energy Balance Around the Ngoring
501 Lake in Source Regions of the Yellow River," *Journal of Glaciology and Geocryology*, vol. 35, no. 6, pp. 1462-
502 1473, 2013.
503 [24]Q. Zhang and X. Cao, "The Influence of Synoptic Conditions on the Averaged Surface Heat and Radiation
504 Budget Energy over Desert or Gobi," *Chinese Journal of Atmospheric Sciences*, vol. 27, no. 2, pp. 245-254, 2003.
505 [25] J. Qiao, "The Temporal and Spatial Characteristics of Atmospheric Boundary Layer and Its Formation
506 Mechanism over Arid Region of Northwest China," *Chinese Academy of Meteorological Sciences*, DA, China,
507 2009.
508 [26] Q. Zhang, J. Zhang, J. Qiao et al., "Relationship of atmospheric boundary layer depth with the thermodynamic
509 processes at the land surface in arid regions of China," *Science China Earth Sciences*, vol. 41, no. 9, pp. 1365-
510 1374, 2011.
511 [27] J. Zhang, Q. Zhang, and C. Tang, "Temporal variety of boundary layer height over deep arid region and the
512 relations with energy balance," *Acta Ecologica Sinica*, vol. 33, no. 8, pp. 2545-2555, 2013.
513 [28] C. Zhao, S. Lv, Z. Li et al., "Numerical Simulation of Influence of Land Surface Thermal Condition on Badain
514 Jaran Desert Atmospheric Boundary Layer Height in Summer," *Plateau Meteorology*, vol. 33, no. 6, pp. 1526-
515 1533, 2014.
516 [29] E. J. Welton, J. R. Campbell, J. D. Spinhirne, and V. S. Scott, "Global monitoring of clouds and aerosols using a
517 network of micropulse lidar systems," *Proc. Lidar Remote Sensing for Industry and Environmental Monitoring,*
518 *Sendai, Japan, SPIE*, Vol. 4153, PP.151–158, 2001.
519 [30] Z. Huang, J. Huang, J. Bi et al. "Dust aerosol vertical structure measurements using three MPL lidars during
520 2008 China‐US joint dust field experiment," *Journal of Geophysical Research: Atmospheres (1984–2012)*,
521 115(D7), 2010.
522 [31] E. Nelson, R. Stull, and E. Eloranta, "A prognostic relation for entrainment zone thickness," *Journal of applied*
523 *meteorology*, vol. 28, no. 9, pp. 885-903, 1989.
524 [32] H. Ding, "Measurements of aerosol vertical profiles and the mixed layer height using a micro pulse lidar,"
525 *Nanjing University of Information science & Technology*, Nanjing, DA, China, 2012.
526 [33] S. Zhao, L. Zhang, Z. Wang et al., "Boundary Layer Height Estimate in summer over the Lanzhou Suburb in
527 Yuzhong Area Using Lidar Measurement and Numerical Model," *Climatic and Environmental Research*, vol. 17,
528 no. 5, pp. 523-531, 2012.
529 [34] R. Wu and Y. Ma, "Comparative Analyses on Radiation Characteristic in Different Areas over the Tibetan
530 Plateau," *Plateau Meteorology*, vol. 29, no. 2, pp. 251-259, 2010.
531 [35] Q. Zhang and S. Wang, "A study on atmospheric boundary layer structure on a clear Day in the arid region in
532 Northwest China," *Acta Meteorologica Sinica*, vol. 66, no. 4, pp. 599-608, 2008.